

A Quantitative Study of Interaction Forces and Friction in Aqueous Colloidal Systems

Adam Feiler, Ian Larson, Paul Jenkins,[†] and Phil Attard*

Ian Wark Research Institute, University of South Australia, Mawson Lakes, Adelaide SA 5095, Australia

Received June 23, 2000. In Final Form: September 25, 2000

Friction-force measurements between a silica sphere and a titanium dioxide wafer in electrolyte solutions were made using an atomic force microscope. The effect of electrical double-layer interactions on the adhesion and the friction force were investigated as a function of pH. In contrast to taking friction measurements in air, conducting the study in aqueous solution has allowed the surface separation, adhesion, and applied force to be controlled independently. Friction was found to be dependent only on the intrinsic force. Friction was seen to be independent of pH. When a force law fitted to the measured data was used, the separation as a function of intrinsic force was likewise found by theoretical calculations to be independent of pH. It was concluded that friction was solely dependent on separation and that the effect of applied force and electrical double-layer interactions served merely to change the separation. In addition, it was proposed that a single layer of unbound water molecules effectively lubricated the surfaces.

Introduction

In recent years direct measurement of frictional force at the molecular scale has become possible, in particular with the use of the atomic force microscope (AFM)¹ and the surface-force apparatus (SFA).² The motivation for studying friction at this scale includes the study of wear,³ the mechanistic understanding of lubrication,⁴ the study of the dependence of friction on adhesion,⁵ the fabrication and maintenance of microelectromechanical systems (MEMS),⁶ and the study of chemical imaging.⁷

Most friction studies are conducted in ambient air. However, the study of friction in the liquid environment is important for three reasons. First, many commercially important applications are conducted in liquid; in these, the control of friction is crucial. These applications include lubrication, wafer cleaning and polishing, mineral processing, grinding, and transport of slurries through pipelines. Second, changing the ionic concentration or pH of a solution allows one to adjust surface properties such as electric charge or adhesion in a controlled and well-defined manner without changing other properties of the measurement. Third, carrying out measurements in a liquid eliminates the effect of capillary forces that hinder and often dominate friction measurements in air.

A number of previous studies measuring friction in aqueous solutions have examined the effect of pH⁸ or

electrode potential^{9–11} on the adhesion and friction force. A comparison of the most relevant work with the present measurements is given in the Discussion section. In this study, the AFM has been used to measure friction between dissimilar oxide surfaces in electrolyte solution under very low applied forces (in the nN range). We investigated the effect of the electrical double-layer interactions on surface separations by measuring the normal force and then by measuring friction as a function of applied force. This strategy made it possible to correlate the friction force with separation and to distinguish between hydrodynamic effects and friction due to contact. The dependence of friction on surface separation at extremely small separations was able to be quantified.

Experimental Section

Reagents. Aqueous solutions of potassium nitrate (KNO₃) were prepared from Analar grade chemicals (BDH) in ultra-high-purity water (surface tension 72.8 mN m⁻¹ and conductivity of 0.5 μS m⁻¹) obtained from an Elga UHQ system. The solution pH was adjusted with 0.01 M HNO₃ or KOH (BDH). The pH of small volumes (15 mL) of the electrolyte solution was measured in a separate plastic container. This precaution was taken to prevent contamination of the solution by the pH electrode.

Silica Spheres. Silica spheres were obtained from Allied Signal, Chicago, Illinois. Scanning electron microscopy was used to size the particles. The typical diameter was found to be 7 μm. AFM imaging at the apex of the spheres over an area of 500 nm² showed the root-mean-square (rms) roughness to be 0.8 nm.

Titanium Dioxide Substrate. A titanium dioxide layer was deposited on the surface of silicon wafers by sputtering. Full details are given elsewhere.¹² X-ray photoelectron spectroscopy (XPS) detected the presence of only Ti and O in a 1:2 ratio (detection limit 0.1 atomic %), indicating that the surface layer was pure titanium dioxide. X-ray diffraction showed that the deposited titanium dioxide was amorphous. Ellipsometry measurements showed the thickness of the titanium dioxide layer to be 25 nm. AFM imaging revealed that the wafers had an rms roughness of 0.3 nm over an area of 1 μm².

* Corresponding author. E-mail, Phil.Attard@unisa.edu.au; FAX, +61 (0)8 8302 3683.

[†] Current address: Unilever Research, Quarry Road East, Port Sunlight, Wirral CH63 3JW, United Kingdom.

(1) Binnig, G.; Quate, C. F.; Gerber, C. *Phys. Rev. Lett.* **1986**, *56*, 930.
(2) Israelachvili, J. N.; Adams, G. E. *J. Chem. Soc., Faraday Trans. I* **1978**, *74*, 975.

(3) Mate, C. M.; McClelland, G. M.; Erlandsson, R.; Chiang, S. *Phys. Rev. Lett.* **1987**, *59*, 1942.

(4) Israelachvili, J. N. *Adhesion, Friction and Lubrication of Molecularly Smooth Surfaces*; Singer, I. L., Pollock, H. M., Eds.; Kluwer Academic Publishers: Dordrecht, The Netherlands, 1992; p 351.

(5) Israelachvili, J. N.; Chen, Y.-L.; Yoshizawa, H. *J. Adhes. Sci. Technol.* **1994**, *8*, 1231.

(6) Bhushan, B. *Tribol. Int.* **1995**, *28*, 85.

(7) Noy, A.; Frisbie, C. D.; Rozsnyai, L. F.; Wrighton, M. S.; Liber, C. M. *J. Am. Chem. Soc.* **1995**, *117*, 7943.

(8) Marti, A.; Hahner, G.; Spencer, N. D. *Langmuir* **1995**, *11*, 4632.

(9) Kelsall, G.; Zhu, Y.; Spikes, H. A. *J. Chem. Soc., Faraday Trans.* **1993**, *89*, 267.

(10) Binggeli, M.; Christoph, R.; Hintermann, H.-E.; Colchero, J.; Marti, O. *Nanotechnology* **1993**, *4*, 59.

(11) Campbell, S. D.; Hillier, A. C. *Langmuir* **1999**, *15*, 891.

(12) Feiler, A.; Jenkins, P.; Ralston, J. *Phys. Chem. Chem. Phys.*, submitted for publication, 2000.

Colloid Probe Preparation. The method for preparing a colloid probe is now well established.^{13,14} Briefly, a silica sphere was attached to the end of a tipless, 200 μm long, wide-legged, silicon nitride cantilever (NP-0 from Digital Instruments). A heat-softening resin (Epikote 1004, Shell) was used for this purpose. An etched tungsten wire, mounted in a micromanipulation arm (Narishige MN-151) attached to a metallurgical microscope (Olympus BH2), was used to attach the particle (colloid probe). Images were projected onto a high-resolution video monitor (Sony PVM2042) via a CCD camera (Sony), and particle alignment was checked using image-analysis software (Galai-Cue 3). The particle radius, R , was measured for each sphere, with the use of a scanning electron microscope (Camscan CS44). Before measurements were taken, the colloid-probe assembly was rinsed with ethanol, dried in a stream of dry nitrogen (filtered to remove particles greater than 50 nm in size), and plasma-cleaned (Harrick Plasma Cleaner/Sterilizer PDC-32) for 1 min. Similarly, the titanium dioxide wafers were cleaned by detergent washing followed by rinsing with high-purity water, ethanol, heptane, and copious amounts of high-purity water. Finally, the wafer was blown dry in a stream of nitrogen and plasma-cleaned for 1 min before immediate use.

AFM Instrument. A Nanoscope III controller and atomic force microscope (Digital Instruments, Santa Barbara, CA) equipped with a fluid cell was used to measure the forces of interaction. Electrolyte solutions (KNO_3 , 10^{-3} M) were introduced into the fluid cell via a syringe and Teflon tubing. The solution was allowed to equilibrate at a temperature of 25 $^\circ\text{C}$ for at least 15 min before measurement.

Force and Adhesion Measurements. Calibration of the cantilever's normal deflection was achieved by measuring the slope of the photodiode detector voltage in the constant compliance region of the force curve while the probe was in contact with the substrate. The z -piezo was calibrated using the method of Jaschke and Butt.¹⁵ The cantilever deflection data were subsequently converted to force (F) as a function of apparent surface–surface separation (h), simply called separation hereafter. The force was converted to the interaction energy or normalized force, i.e., F/R , employing the Derjaguin approximation for sphere–flat interactions.¹⁶ Force-separation profiles were analyzed using the AFM Analysis software package.¹⁷ The cantilever's normal spring constant was determined by measuring the resonant frequency of the cantilever before and after attachment of tungsten spheres.¹⁸ A minimum of five tungsten spheres per cantilever were used. The normal spring constants were found to vary from 0.09 to 0.11 ± 0.01 N m^{-1} . The scan range and scan rate were 1 μm and 0.5 Hz, respectively.

Friction Measurements. Friction force measurements were made in “friction mode”. The titanium dioxide flat substrate was moved back and forth in a direction perpendicular to the cantilever's long axis. The completion of one scan in each direction formed a friction loop. The lateral deflection signal was measured as a function of substrate movement over a fixed distance of 500 nm and at a frequency of 1 Hz. The recently developed method of Feiler et al.¹⁹ was used to measure the cantilever's torsional spring constant and, simultaneously, calibrate the photodiode response to the angular deflection of the cantilever. In this nondestructive technique, a glass lever is glued to the tip of the cantilever,²⁰ and the vertical and lateral deflection voltage signals are recorded²¹ as a flat substrate is brought in contact with the lever. The lever is attached in the plane of the cantilever but

orthogonal to the cantilever's long axis. The torque, τ , applied to the lever of length L , is given by $\tau = FL$, where F is the normal force exerted by the substrate. The torque, which twists the cantilever, is measured by a change in the vertical, ΔV_{vert} , and the lateral, ΔV_{lat} , voltage signal. The voltage signals, which are recorded simultaneously, show that a change in the lateral deflection corresponds directly to a change in the vertical deflection. The calibration factor, γ , which was obtained from the slope of a $V_{\text{vert}}/V_{\text{lat}}$ plot, the constant compliance slope of normal deflection, and the normal spring constant, converts the lateral voltage signal to the applied torque

$$\tau = \gamma \Delta V_{\text{lat}} \quad (1)$$

It is then a simple matter to convert the voltage signal to a friction force, F_f

$$F_f = \frac{\gamma V_{\text{FFM}}}{d} \quad (2)$$

where V_{FFM} is the lateral deflection signal, taken as half the voltage difference between the trace and retrace curves in a typical friction loop, and d is the height of the colloid probe.

The friction force was measured as a function of decreasing applied force. As shown later, the force curves at high pH reveal that there can be two possible separations for a given force. By starting the friction measurements at high applied force and decreasing the force systematically, we ensured that the surfaces were always at the closer of the two separations. We controlled the applied force in friction mode by adjusting the setpoint voltage. Before friction measurements were made, force-separation curves were captured and the setpoint adjusted such that zero force at large separations corresponded to 0 V. The friction force was calculated from an average of at least four separate friction measurements.

Deformation Calculations. The elastic deformations of the sphere and the substrate under the influence of the applied force and their adhesion were calculated according to the algorithm of Attard and Parker.^{22,23} This algorithm gives the shape of the deformed surfaces and the local pressure, using a self-consistent iterative technique. In previous work, the pressure arising from model surface forces was used.^{22,23} In this work, the actual pressure, derived from fitting the measured force data at each pH, is used in the deformation calculations.

According to the Derjaguin approximation, the force, F , measured between a sphere and a flat is related to the interaction free energy per unit area, $G(h)$, between planar walls by

$$G(h) = \frac{F(h)}{2\pi R} \quad (3)$$

Hence, the net pressure, p_s , which is simply the derivative of the free energy, may be extracted from the experimentally measured force

$$p_s(h) = \frac{-1}{2\pi R} \frac{\partial F(h)}{\partial h} \quad (4)$$

The total fitted force is

$$F(h) = F_{\text{vdw}}(h) + F_{\text{edl}}(h) \quad (5)$$

where F_{vdw} comprises the force due to attractive van der Waals interaction and also the short-range repulsion that is derived from the Lennard-Jones 6–12 potential

$$F_{\text{vdw}}(h) = \frac{AR}{6h^2} \left(\frac{z^6}{4h^6} - 1 \right) \quad (6)$$

where $R = 3.5 \mu\text{m}$ for the silica sphere, the Hamaker constant

(13) Ducker, W. A.; Senden, T. J.; Pashley, R. M. *Nature* **1991**, *352*, 239.

(14) Ducker, W. A.; Senden, T. J.; Pashley, R. M. *Langmuir* **1992**, *8*, 1831.

(15) Jaschke, M.; Butt, H.-J. *Rev. Sci. Instrum.* **1995**, *66*, 1258.

(16) Israelachvili, J. N. *Intermolecular & Surface Forces*, 2nd ed.; Academic Press: London, 1992.

(17) Ip, L.; Chan, D. Y. C.; Venters, S. *AFM Analysis*, version 2; Department of Mathematics, University of Melbourne: Melbourne, Australia, 1994.

(18) Cleveland, J. P.; Manne, S.; Bocek, D.; Hansma, P. K. *Rev. Sci. Instrum.* **1993**, *64*, 402.

(19) Feiler, A.; Larson, I.; Attard, P. *Rev. Sci. Instrum.* **2000**, *71*, 2744.

(20) Toikka, G.; Hayes, R. A.; Ralston, J. *J. Adhes. Sci. Technol.* **1997**, *11*, 1479.

(21) Bogdanovic, G.; Meurk, A.; Rutland, M. W., *Colloids Surf. A*, submitted for publication, 1999.

(22) Attard, P.; Parker, J. L. *Phys. Rev. A* **1992**, *46*.

(23) Parker, J. L.; Attard, P. *J. Phys. Chem.* **1992**, *96*, 10398.

$A = 1.4 \times 10^{-20}$ J,²⁴ and $z = 0.5$ nm. The latter quantity characterizes the range of the soft, short-range repulsion, and at some level it approximates the Born repulsion. In practice, the actual value of z is of little importance. Because the repulsion is so steep for $h < z$, experimentally it is indistinguishable from a hard-wall repulsion. Hence, the experimental separations were shifted by z , so what is called contact in the measured force-separation curves corresponds to $h = 0.5$ nm in the calculated results. These parameters were fixed throughout and not varied in the fitting procedure.

The remainder of the measured force, which includes the electrical double-layer, hydration, and structural force, was fitted with the form

$$F_{\text{edl}}(h) = \left(a + \frac{b}{h} + \frac{c}{h^2} \right) e^{-\kappa h} \quad (7)$$

where the Debye length was fixed at $\kappa^{-1} = 9.65$ nm for the 10^{-3} M electrolyte solution. The three parameters (a , b , and c) in the prefactor were obtained by a least-squares fit to the measured force curves (shown later); care was taken to ensure that the adhesion obtained in the separation data was reproduced by the fit. The values of these parameters varied with pH, which reflects the dependence of the surface charge on the concentration of the potential-determining ion. The prefactor is a convenient functional form that has enough flexibility to give an accurate fit to the experimental data, particularly at short range. It includes hydration and steric effects that are not already accounted for in the Born repulsion. Apart from the first term that dominates at long-range, the prefactor should not be considered to imply any statement about the form of the actual double-layer interactions in the present system.

The bulk material properties of the sphere and substrate were considered identical to those of silica. The 25-nm-thick coating of the titanium dioxide on the substrate is not expected to affect its elastic properties. Values of Young's modulus, $E = 7.2 \times 10^{10}$ J m⁻³,²⁵ and Poisson ratio, $\nu = 0.25$,²⁶ were used. These values are those for a relatively rigid solid. Elastic hysteresis, found by Attard and Parker for very soft solids, was not present in the current system.^{22,23} The numerical calculations may be regarded as exact because their accuracy is several orders of magnitude greater than that of the experimental data.

Results and Discussion

Force Measurements. The force-versus-separation curves for the approach of a titanium dioxide wafer toward a silica colloid sphere, over a range of pH values, are presented in Figure 1. It is evident that the surface potentials and, hence, surface chemistry change significantly with pH. In agreement with other studies on the silica–titanium dioxide system,^{12,24,27} the force of interaction is seen to be dominated, at all but very small separations, by the interaction of the electrical double layers of the approaching surfaces. The interaction changes from a long-range repulsion at high pH to an attraction at low pH. This is consistent with the known variation of surface potentials as a function of pH. Silica has an isoelectric point (iep) at \sim pH 2,²⁸ and thus is expected to have a negative potential across the pH range studied. The iep of the titanium dioxide wafer was measured to be \sim pH 4.5.¹² At pH values above its iep, the titanium dioxide wafer has a negative potential and the electrical double-layer interaction between the two surfaces is repulsive. At pH values between the two iep's,

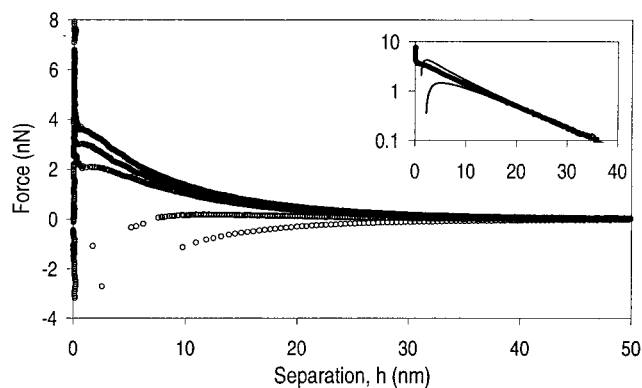


Figure 1. Force-distance curves for the approach of a silica sphere ($R = 3.5 \mu\text{m}$) and a titanium dioxide wafer as a function of pH in a background electrolyte of 10^{-3} M KNO_3 . The curves correspond to, from top to bottom, data at pH 8, 7, 6, 5, and 4. The inset shows the data at pH 8, along with the constant-charge (top line) and constant-potential (bottom line) solutions to the nonlinear Poisson–Boltzmann equation. The theoretical fits were performed using a Hamaker constant of 1.4×10^{-20} J,²⁴ and surface potentials of $\Psi_{\text{SiO}_2} = -50$ mV and $\Psi_{\text{TiO}_2} = -43$ mV. Table 1 lists the fitted potentials at the other pH values.

Table 1. Surface-Force and Friction Properties

pH	$\Psi_{\text{SiO}_2}^a$ (mV)	$\Psi_{\text{TiO}_2}^a$ (mV)	F_{detach}^b (nN)	μ^c
4	-25	+10	-10.5	0.73
5	-30	-20	-4.4	0.43
6	-50	-38	+1.4	0.80
7	-51	-40	+2.6	0.66
8	-53	-43	+3.5	0.70

^a The diffuse layer potentials are accurate to within ± 3 mV.

^b The detachment force varied by 10% between different force curves.

^c The friction coefficient is accurate to within ± 0.01 .

when the titanium has a positive surface potential, the double-layer interaction is attractive. The total force of interaction can be modeled by the combination of van der Waals and electrical double-layer interactions proposed by the Derjaguin–Langau–Verwey–Overbeek (DLVO) theory of colloid stability.^{29,30} The diffuse layer potentials were obtained by fitting the data with numerical solutions of the nonlinear Poisson–Boltzmann equation. The inset in Figure 1 shows data at pH 8 with the fitted DLVO model calculated under constant-charge and constant-potential-boundary conditions. The data lies between the two extremes defined by the boundary conditions at all pH values, even down to small separations. However, the data is described better by the constant-charge condition. The measured diffuse layer potentials at all pH values are shown in Table 1. With the exception of the pH 8 force curve, a jump into contact, due to van der Waals attraction, was detected at small separations. As will be discussed in the following section, the surfaces do come into contact at all pH values. However, at high pH, an applied force is necessary to force the surfaces together. At low pH, the jump into contact is spontaneous once the force gradient exceeds the cantilever stiffness.

Before the retraction data is discussed, it is necessary to define the terminology used to describe the forces acting during separation of the surfaces. By introducing the term “detachment force”, F_{detach} , rather than “pull-off force”, to describe the force needed to separate the surfaces, we hope to avoid confusion when discussing the separation

(24) Larson, I.; Drummond, C. J.; Chan, D. Y. C.; Grieser, F. *J. Phys. Chem.* **1995**, *99*, 2114.

(25) Sosman, R. B. *The Properties of Silica*; The Chemical Catalog Company: New York, 1927.

(26) Anderson, H. L. *A Physicist's Desk Reference Physics Vade Mecum*, 2nd ed.; American Institute of Physics: New York, 1981.

(27) Hu, K.; Fan, F.-R. F.; Bard, A. J. *J. Phys. Chem. B* **1997**, *101*, 8298.

(28) Parks, G. A. *Chem. Rev.* **1965**, *65*, 177.

(29) Verwey, E. J.; Overbeek, J. T. *Theory of Stability of Colloidal Dispersions*; Elsevier: Amsterdam, 1948.

(30) Derjaguin, B.; Landau, L. *Acta Physicochem. USSR* **1941**, *14*, 633.

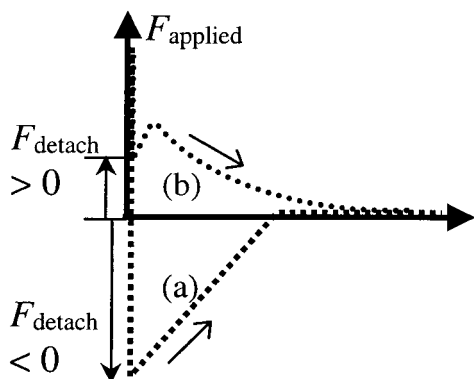


Figure 2. Schematic of typical force curves during the separation of two (a) attractive surfaces with a negative F_{detach} and (b) repulsive surfaces, separating in the presence of a nonzero applied force, with a positive F_{detach} . The magnitude of the applied force is determined from the deflection and normal spring constant of the cantilever.

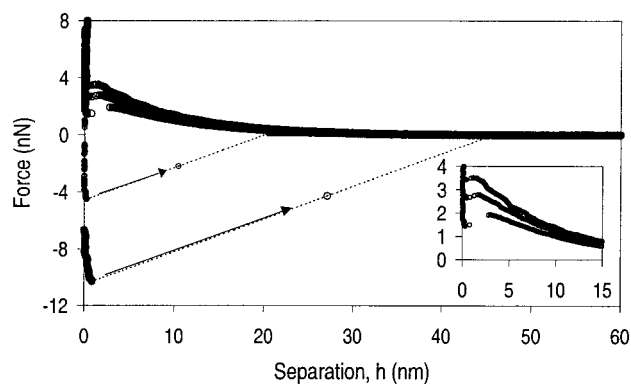


Figure 3. Force-distance curves for the retraction of a titanium dioxide wafer from a silica sphere ($R = 3.5 \mu\text{m}$) as a function of pH in 10^{-3} M KNO_3 . The curves correspond to, from top to bottom, data at pH 8, 7, 6, 5, and 4. The inset shows the data at pH 8, 7, and 6 for small separations.

of *repulsive* surfaces. Figure 2 shows a schematic of two typical retrace force curves. The applied force, F_{applied} , is the force exerted by the cantilever and is determined by the normal spring constant and the cantilever deflection. For curve (a), a strong attraction exists between the surfaces, and they remain in contact even when the applied force is zero. A negative F_{detach} indicates that a tensile force is needed to separate the surfaces. In curve (b) the force is dominated by a repulsive interaction, and the surfaces spontaneously separate even in the presence of an applied force. In this case, F_{detach} is positive, and it is a measure of the force at which the repulsive interactions exceed the applied force. In other words, for attractive or repulsive interactions, F_{detach} is the smallest applied force needed to keep the surfaces in contact. In the case of adhesion, when the applied force goes below zero before the surfaces separate, F_{detach} is negative. Conversely, when the surfaces separate at a force greater than zero, F_{detach} is positive.

The force curves upon retraction are shown in Figure 3 for the same conditions as in Figure 1. The data starts with the surfaces in contact under the influence of the maximum applied force. As the substrate is retracted, the applied force is decreased and, at a given force F_{detach} , the surfaces separate. At pH 4, a strong attraction exists between the oppositely charged surfaces, and F_{detach} is -10.5 nN. At pH 5, an adhesion is also measured, although it is significantly less than that at pH 4 because close to the iep of titanium dioxide, the electrostatic interaction

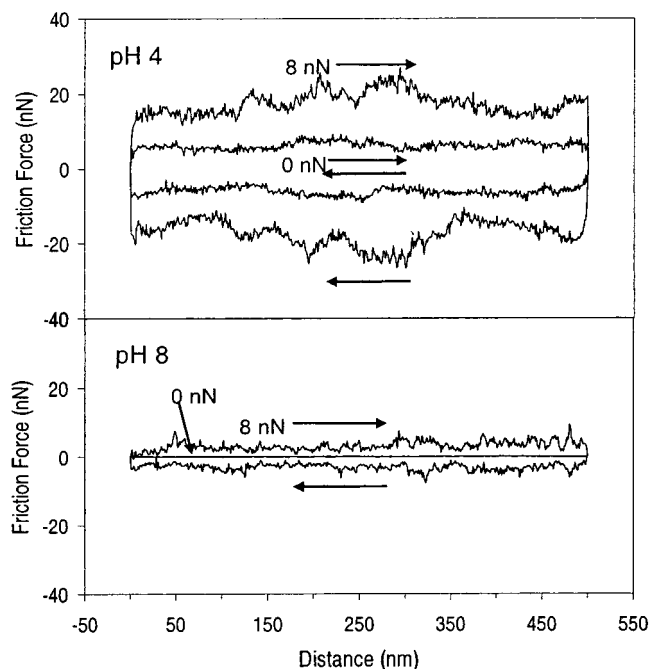


Figure 4. Typical friction-force data, plotted as friction force against substrate movement, for pH 4 (upper) and pH 8 (lower) in 10^{-3} M KNO_3 . The arrows indicate the direction of substrate movement, with one trace and retrace scan completing the friction loop. For both pH values, the outer loop is the data collected with an applied force of 8 nN, and the inner loop (or line, as in the pH 8 case) is the data collected with zero applied force. At pH 8, the friction is undetectable with zero applied force, whereas friction is still detectable at pH 4 under the same condition.

is diminished. At pH 5, F_{detach} is -4.4 nN. At higher pH, electrostatic repulsion dominates the interaction force and causes the surfaces to separate even when there is still a significant applied force. The inset in Figure 3 shows the data at high pH for small separations. At pH 6, partial adhesion is evident from the jump out of contact, despite the net repulsive interaction that dominates the force at nonzero separation. At still higher pH values, even less adhesion is detected. In fact, the surfaces separate readily under the influence of the repulsive force. The measured values of F_{detach} at all pH values are shown in Table 1.

The variation of F_{detach} with pH and its change in sign near the iep of titanium dioxide indicate that F_{detach} is dependent on the properties of the electrical double layer on each surface. It is most likely that the van der Waals force is invariant with pH¹⁶ and that the change in the double-layer interaction (and possibly other effects such as hydration) with pH gives the variation in adhesion. In fact, when F_{detach} is plotted as a function, $\psi_{\text{SiO}_2} \times \psi_{\text{TiO}_2}$, it lies exactly on a straight line (not shown), proving the invariance of the van der Waals force across the pH range studied. The implication of this result is currently under further investigation.

Friction-Force Loops. Figure 4 shows examples of typical friction loops taken with no applied force and with an applied force of 8 nN at both pH 4 and 8. For both pH values, the friction force decreases markedly when the applied force is removed. For a given applied force, the friction at pH 4 is larger than at pH 8. In fact, the friction force at zero applied force is larger at pH 4 than in the presence of an 8 nN applied force at pH 8. At zero applied force, no friction is detectable at pH 8. This observation is consistent with the force curve in Figure 3, which shows that, at pH 8 with no applied force, the surfaces are

separated because of the electrical double-layer repulsion. In contrast, at pH 4 the surfaces are in contact at zero applied force, and a friction force is measured.

The "spiky" noise in the data in Figure 4 was evident in all the friction loops. At high applied forces, there tended to be low-frequency noise with high frequency noise superimposed. At low applied force, the noise was greatly reduced. For high applied forces, the low-frequency noise seen in the trace scan was mirrored in the retrace scan, indicating that this noise probably was due to topographical effects (e.g., surface roughness or chemical heterogeneity on the 10–100 nm scale). The high-frequency noise could also be due to topography, or it might simply be due to electrical noise. As is discussed later in this paper, the resolution of the data points is of the order of nanometers, and so the noise detected in these friction loops certainly is not due to atomic-scale stick–slip behavior.^{3,31}

It is worth noting that a static friction force was not detected in any of the friction loops. That is, no initial large peak in the friction loops was measured; the first data point had a value similar to those of the other data points in the loop. In studies of friction in air,^{4,32,33} static friction is observed as a large peak in the first few data points, i.e., in the period where the surfaces are pinned in the presence of a shear force. Once motion is initiated, the dynamic friction force is often much less than the static friction, because the force needed to maintain motion is less than that needed to initiate sliding.^{4,32} In the present study, the minimum amount of static friction that can be detected is limited by the resolution of the data. It depends on the number of data points that are collected during one scan and also on the torsional spring constant of the cantilever. For static friction to be detected, the tip of the probe must be pinned to the substrate for at least the distance that the substrate moves between successive data points. Because static friction was not detected, if it is present, it must be less than the force required to pin the tip between data points. It is therefore possible to calculate an upper limit for the static friction present in this system. In this study, 512 data points were collected over a scan size of 500 nm, which means that the substrate moved 0.97 nm between data points. The angular deflection of the cantilever, $\Delta\theta$, and the friction force, F_f , are related to the torque, τ .¹⁹

$$\tau = F_f d = k_\theta \Delta\theta \quad (8)$$

and, hence

$$F_f = \frac{k_\theta \Delta\theta}{d} = \frac{k_\theta \Delta x}{d^2} \quad (9)$$

where $d = 7 \mu\text{m}$ is equal to the height of the colloid probe and $k_\theta = 2 \times 10^{-9} \text{ N m}$ is the torsional spring constant of the cantilever.¹⁹ A lateral movement of the probe of $\Delta x = 0.97 \text{ nm}$ would result in an angular deflection of the cantilever of $\Delta\theta = 1.4 \times 10^{-4} \text{ rad}$ and a force of 40 nN. In other words, since static friction was not detected in the present study, it must be less than 40 nN. The largest dynamic friction measured was $\sim 30 \text{ nN}$. The fact that in this study the static friction, if any, is not much larger than the dynamic friction is not unreasonable. In air, the action of capillary forces often dominates static friction.

(31) Ruan, J.; Bhushan, B. *J. Appl. Phys.* **1994**, *76*, 8117.

(32) Yoshizawa, H.; Chen, Y.-L.; Israelachvili, J. *J. Phys. Chem.* **1993**, *97*, 4128.

(33) Persson, B. N. J. *Theory of Friction: Friction Dynamics for Boundary Lubricated Surfaces*; Bhushan, B., Ed.; Kluwer Academic Press: Dordrecht, The Netherlands, 1997; p 555.

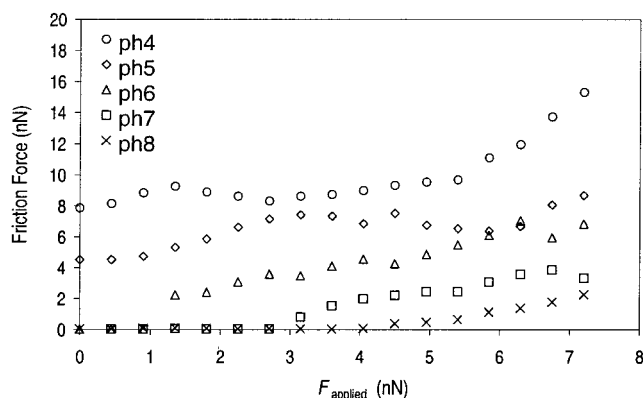


Figure 5. Friction force as a function of applied force in 10^{-3} M KNO_3 . At pH 4 and 5, friction is nonzero at all applied forces. At pH 6, 7, and 8, the friction becomes undetectable (at F_{detach}), even in the presence of an applied force.

tion,^{4,16,34,35} whereas in liquid the present results show that this force is largely eliminated.

Friction-Force Measurements. The measured friction as a function of applied force, over the range of pH values studied, is shown in Figure 5. At any given applied force, the friction is highest at pH 4 and decreases uniformly with increasing pH. At low pH, friction is measured even at zero applied force. Conversely, at high pH the friction force becomes zero before the applied force is fully removed. The nonzero friction at zero applied force at pH 4 and 5 can be rationalized in terms of the adhesion seen in Figure 3, because at low pH, a negative F_{detach} confirms that the surfaces are still in contact at zero applied force.

At pH 6 and above, where there is a repulsive electrical double-layer interaction, a friction force exists only when the surfaces are in contact with an applied force greater than F_{detach} . For positive applied forces less than F_{detach} , the interaction is dominated by repulsive electrical double-layer forces and the surfaces are separated. In these cases the friction is zero. In fact, at each pH, the friction force becomes zero exactly at F_{detach} , which is the applied force at which the surfaces separate in Figure 3. In other words, friction becomes zero when $F_{\text{applied}} = F_{\text{detach}}$. One can conclude that contact is an essential requirement for friction.

Clearly, the electrical double-layer interaction is acting as a component of the applied force in determining the friction. It also contributes to F_{detach} , as shown by the pH dependence. The intrinsic force, $F_{\text{intrinsic}}$, which is defined as

$$F_{\text{intrinsic}} = F_{\text{applied}} - F_{\text{detach}} \quad (10)$$

will now be shown to be largely independent of pH and the electrical double layer. $F_{\text{intrinsic}}$ can be calculated simply using F_{detach} measured from the retract curves. It is apparent that, for attractive electrical double-layer interactions, the intrinsic force is larger than the applied force by $|F_{\text{detach}}|$. For repulsive interaction, $F_{\text{intrinsic}}$ is less than the applied force by $|F_{\text{detach}}|$. In Figure 6, the friction-force data are plotted against $F_{\text{intrinsic}}$. The result is remarkable. The data points for all pH values lie on a single curve. In other words, when plotted as a function of $F_{\text{intrinsic}}$, friction is not directly affected by pH. In traditional representations of friction versus applied force (see Figure 5), this pH independence cannot be perceived.

(34) Bhushan, B. *Wear* **1999**, *225–229*, 465.

(35) Ando, Y.; Ino, J. *Wear* **1998**, *216*, 115.

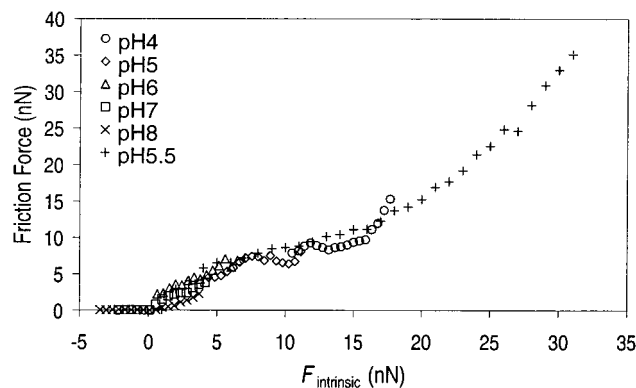


Figure 6. Friction force against intrinsic force, $F_{\text{intrinsic}}$. The data points measured at pH 5.5 were measured with a different sphere and substrate over a larger force range, with a maximum applied force of 33 nN. The other data points are the same as plotted in Figure 5 and correspond to a maximum applied force of 8 nN. $F_{\text{intrinsic}}$ was calculated according to eq 10 using the detachment force measured in Figure 3. The data points for all pH values lie on a single curve. Friction becomes undetectable when the intrinsic force becomes zero.

The data collected over the larger force range in Figure 6 are particularly convincing as they overlay all the other data at other pH values.³⁶

In Figure 6, friction becomes zero when $F_{\text{intrinsic}}$ is zero, and, as the data points taken at high pH show, no friction is measured below zero intrinsic force. This result is important because it shows that, in this system, friction is wholly dependent on the intrinsic force acting between the two surfaces. Surprisingly, it appears that a single experimentally measurable parameter, viz. F_{detach} , adequately accounts for variation of the intrinsic force with pH due to electrical double-layer interactions, hydration and structural forces, and even specific chemical interactions between the surfaces.

The data shows an increase in friction force with increasing $F_{\text{intrinsic}}$. However, the change of friction with changing $F_{\text{intrinsic}}$ or F_{applied} is not linear. Traditionally, a linear dependence of friction with applied force is assumed in order to satisfy Amonton's law, which states that $F_f = \mu \times F_{\text{applied}}$, where F_f is the friction force and μ is the coefficient of friction. Alternatively, a nonconstant coefficient of friction has been suggested for cases in which friction varies with applied force.³² The coefficient is then defined as $\mu = dF_f/dF_{\text{applied}}$. Berman and Israelachvili³⁷ suggest that a nonconstant friction coefficient arises when the contact area, which ultimately determines the magnitude of the friction, varies nonlinearly with applied force. Ando³⁸ invokes Johnson, Kendall, Roberts (JKR) theory to rationalize a force-dependent attraction between a sphere and a flat that results in an increasing friction coefficient with decreasing applied force. In the present system, a nonconstant coefficient of friction seems more applicable. The friction coefficients measured at each pH value, averaged over the nonzero data, are shown in Table 1. Clearly, a single value for the friction coefficient for all pH values is not appropriate. However, the variation of

(36) The data measured over the larger force range was taken at pH 5.5 with a different sphere ($R = 3 \mu\text{m}$) and substrate. At this pH, the detachment force was very close to zero nN, and in this case $F_{\text{intrinsic}} = F_{\text{applied}}$. The maximum applied force over the larger range was 33 nN compared to about 8 nN for the other data.

(37) Berman, A.; Israelachvili, J. N. *Control and Minimization of Friction via Surface Modification*; Bushan, B., Ed.; Kluwer Academic Press: Dordrecht, The Netherlands, 1997; p 317.

(38) Ando, Y. *Effect of Adhesion Force on Friction under Low Normal Load*; Mechanical Engineering Laboratory: Ibaraki, Japan, 1998.

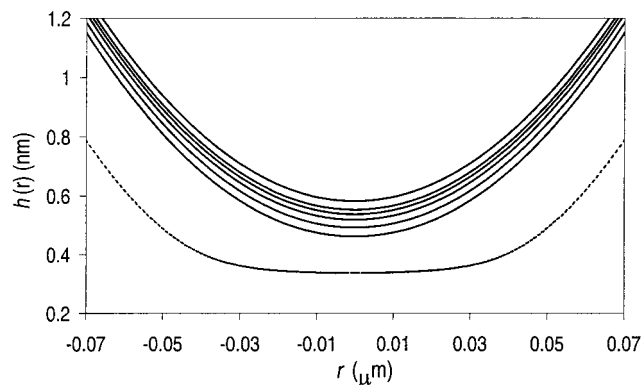


Figure 7. Calculated surface shape of the colloid probe sphere at each pH for an applied force of 5 nN. The distance from the central axis of the sphere is r . The curves correspond to, from top down, pH 8, 7, 6, 5, and 4. Also plotted is a calculated surface shape for an applied force of 720 nN (bottom dashed curve).

μ with pH is simply a consequence of extracting different regions of the friction curve to calculate μ . The fact that the data measured over the larger force range overlie the other data measured at different pH values indicates that the variation in μ is a true reflection of the change of friction with intrinsic force. This fact reinforces the idea that the friction is not a linear function of applied force and that friction is independent of pH and surface charge. It suggests that friction is dominated by the energy-transfer processes characteristic of the bulk solid surfaces, and that these transfer processes change with intrinsic force.

Deformation and Contact-Force Calculation. To ascertain more precisely the effect of surface forces on the interaction between the sphere and the substrate, we applied the elastic deformation algorithm of Attard and Parker^{22,23} to the measured force-separation data. Equations 6 and 7 were fitted to the force data in Figures 1 and 2. From this expression, the force was differentiated analytically to obtain the net pressure, $p_s(h)$, acting on the two surfaces as a function of actual separation (see eqs 3 and 4). The shape of the sphere, the total force, and the actual separation were calculated as a function of nominal separation at each pH. Figure 7 shows the surface profiles for the sphere at each pH value with an applied force of 5 nN. The cross-sectional profiles appear parabolic rather than circular because of the asymmetric scale of the two axes (the x -axis is in units of μm , whereas the y -axis is in units of nm). The profiles are virtually indistinguishable from the corresponding profiles for infinitely rigid bodies (not shown). Under this small applied force, the deformation of the sphere is almost undetectable. It is not until much larger forces are applied that a significant deformation is seen. The surface profile predicted at an applied force of 720 nN shows a marked deformation leading to a flattening of the contact region and a smooth transition to the undeformed shape away from contact. It is worth noting that the van der Waals force and elasticity of the present system correspond to a value of Attard and Parker's²² dimensionless parameter of $\sigma = 2.4 \times 10^{-3}$. Because this value is much less than 1, there is no adhesion hysteresis due to elasticity, nor is there a jump into contact due to elastic instability.²² In the language of contact mechanics, the present system lies at the Derjaguin, Muller, Toporov (DMT), end of the elastic adhesion spectrum.

The main effect of pH is to change the distance of closest approach for a given applied force. As might be expected, for a given applied force, the surfaces are closer together

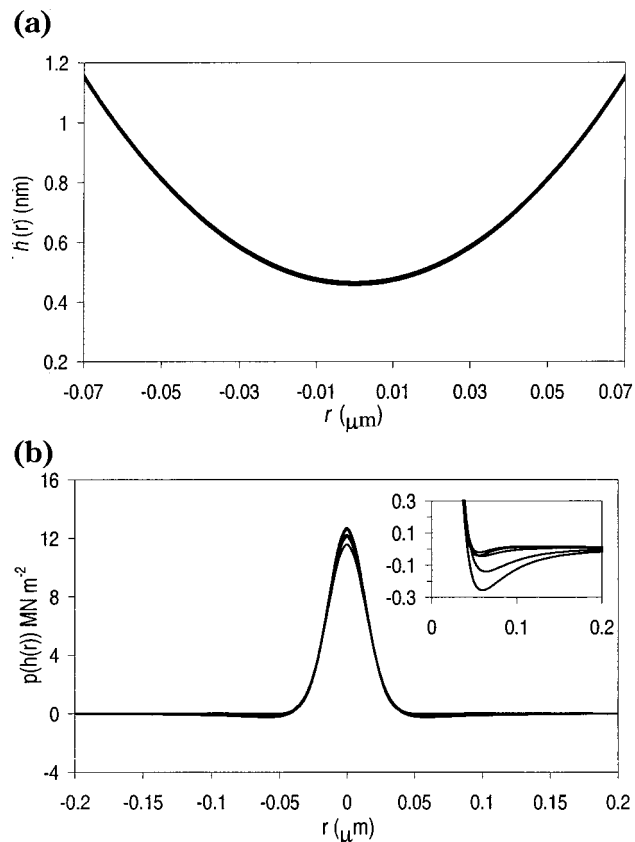


Figure 8. (a) Surface profiles for the colloid probe sphere, at different pH values, calculated for an intrinsic force of 15 nN. The curves represent the data at, from top to bottom, pH 8, 7, 6, 5, and 4. The surface profiles are virtually indistinguishable from each other. (b) The corresponding pressure-distribution profiles for the curves. The pressure profiles are very similar at each pH. The deviation in the profiles with pH, shown in the inset, is a consequence of the variation of the force law at different pH values. In fact, the surface pressure will be dominated by the central pressure, which is almost identical at each pH.

at low pH (when there is an additional attractive double-layer interaction) than at high pH (when repulsive electrostatic interactions are present). As mentioned following eq 7, the onset of the short-range repulsive force was modeled at a surface separation of $z = 0.5$ nm. In Figure 7, for an applied force of 5 nN at pH 4, the separation $h(0) = 0.46$ nm, which implies that the short-range Born repulsion dominates the interaction force at this separation. Conversely, at pH 8, the distance of closest approach for the given applied force is $h(0) = 0.58$ nm, which corresponds to the attractive part of the van der Waals force. Hence, one could possibly conclude that the reason friction increases with decreasing pH, for a given applied force, is simply that the surfaces are in closer proximity. As will be shown later, the dependence of friction on separation can be tested when values for the surface separations are extracted from theoretical fits to the measured force curves.

As discussed earlier, the friction force is the same for a given value of $F_{\text{intrinsic}}$ at all pH values studied. In Figure 8(a), the surface profiles at different pH values are plotted for a value of $F_{\text{intrinsic}}$ of 15 nN. Note that this value of $F_{\text{intrinsic}}$ corresponds to an applied force of 5 nN at pH 4, conditions for which the surface profile has already been plotted in Figure 7. The surface separation is now almost the same at each pH. Figure 8(b) shows the pressure profiles corresponding to Figure 8(a). The pressure profiles

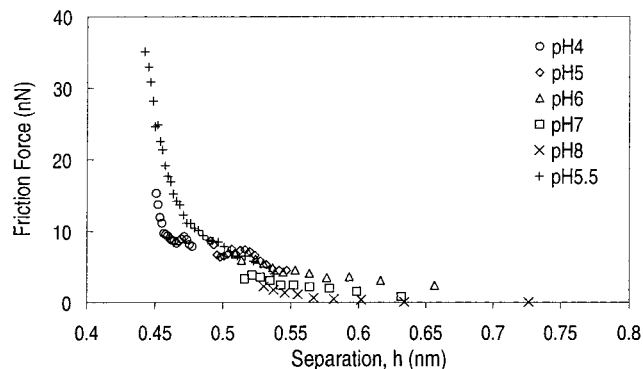


Figure 9. Friction force as a function of surface-surface separation between the colloid probe and flat substrate. The surface-surface separation has been calculated from the theoretical fits to the measured force curves based on model smooth surfaces.

are very similar at each pH. The pressure is highly compressive in the center and decays smoothly away from the axis. However, as the inset shows, the pressure profiles are not identical. At around $0.05 \mu\text{m}$, the pressure changes from repulsive to attractive in agreement with a DMT or JKR-type interaction. The variation in the pressure profiles is a consequence of the variation in the force laws with pH. However, the magnitude of the pressure at this distance from the center is small, and its variation with pH is insignificant compared to relative invariance of the pressure at the central axis. Thus, for a given intrinsic force, the pressure is dominated by the repulsive regime near the center and is almost independent of pH.

Friction Versus Separation. Figure 6 showed that F_{detach} corrected the experimental data to give friction independent of pH. Similarly, Figure 8 showed that F_{detach} corrected the theoretical data to give separations independent of pH. This invariance, common in the two approaches, gives confidence in both the utility of F_{detach} and the applicability of the theoretical calculations. It further suggests that separation is the proximate determinant of friction, and also that the change in friction with applied force occurs because of the change in separation. Accordingly, the measured friction has been plotted as a function of separation in Figure 9.

Given that applied force is a steeply increasing function of separation, and because it can be measured accurately, the fitted-force law can be used to extract the separation corresponding to the applied force at which the friction was measured. These separations are given at much higher resolution than can be measured directly. As with all AFM measurements, some ambiguity exists in the measured zero of separation. Traditionally, the onset of the constant-compliance region is defined as zero separation. The determination of separation is therefore limited to the accuracy with which the constant-compliance region can be identified. For all the data presented here, the maximum variation of data points within the constant-compliance regime was 0.2 nm. Because the fitting procedure averages the data over all the points, the uncertainty in ascribing position is reduced. So although some ambiguity exists in the absolute separations, within the validity of the fitted functional form, the relative separations for each curve in Figure 9 are likely to be quantitatively accurate.

Figure 9 shows that friction increases rapidly with decreasing separation. The trend in the data is very similar at each pH, and again, the data taken over a larger force range overlay the other data. When presented in this form,

the rapid nonlinear increase in $F_{\text{intrinsic}}$ at very small separations becomes clear.

In view of the fitted-force law, separations greater than 0.5 nm correspond to the attractive part of the Lennard-Jones interaction (van der Waals attraction), whereas separations less than 0.5 nm correspond to repulsion between surface atoms, in part because the overlap of the outer electronic orbitals (Born repulsion). In the Lennard-Jones model, the separation is measured between the centers of the surface atoms. It is a moot point whether the surface atoms are the atomic constituents of SiO_2 and TiO_2 or are instead a monolayer of bound and immobile water molecules that hydrate the solid and are not removed by the applied forces. The present measurements cannot distinguish these two cases. However, they do show that *if* there is such a bound monolayer, it does not act as a lubricant, and that measurable friction still occurs.

Although the friction is obviously large when the surfaces interact via the Born repulsion, it is also nonzero when they interact only via van der Waals attraction. This is reasonable because friction represents the energy dissipation due to proximal motion of two surfaces, and it therefore requires some mechanism for energy transfer from one surface to another. The van der Waals interaction provides such a mechanism, albeit less efficiently than when the surfaces are in closer contact. Nevertheless, a nonzero friction results. In view of this fact, we can now give a more precise meaning to contact than that used earlier. As discussed above, friction was said to be nonzero when the surfaces were in contact, with contact defined in terms of experimentally resolvable separations. Now, contact may be defined as occurring whenever individual atoms on opposite surfaces interact with a strength greater than the thermal energy, kT . In the Lennard-Jones model, this occurs at about 0.7 nm. In other words, assuming "soft" contact (the extent of the soft, short-range repulsion and Born repulsion, as described in the Experimental Section) corresponds to separations out to 0.5 nm, friction could still exist up to 0.2 nm beyond the point of soft contact.

Evidently, the resolution of the separation scale is much finer than the measured roughness of the surfaces. The calculations have been performed for the simplest model, which is an idealized, mathematically smooth surface. The measured rms roughnesses were 0.8 and 0.3 nm for the silica sphere and the titanium dioxide wafer, respectively. However, because the surface roughness will not vary with pH, only a constant systematic error will be introduced by neglecting it. The calculated invariance of separation with $F_{\text{intrinsic}}$ will not change if roughness is included. It is also possible that the asperities deform because of the large local pressures, making the surfaces smoother when in contact. This will reduce the ambiguity in assigning absolute surface position. Of course, in the real system, it is most likely to be the interacting asperities that dominate friction. In view of the steep increase in repulsion at small separations, it is possible that the increase in friction is due simply to the increasing number of asperity contacts.

Discussion. Several investigators have studied friction in systems with electrical double-layer forces.^{8,9,11} In contrast to the present study, Kelsall et al.⁹ and Campbell and Hillier¹¹ assumed a linear dependence of friction with applied force and observed a charge-dependent friction coefficient that varied with changes in pH⁹ or electrode potential.¹¹ Kelsall et al. attributed this pH dependence to changes in the electrical double-layer interactions in microgaps within the contact region. These authors described a simple model that invoked the average gap

thickness and an effective contact area, neither of which can be measured experimentally. Campbell and Hillier reached essentially the same conclusions and proposed a similar model, which also invokes parameters that cannot be measured. In the appendix to this work, we show that the electric double-layer forces are dominated by contributions from outside of the contact region. Hence, it is difficult to justify the assertion that it is the electrical double-layer interactions within the microgaps that determine friction.

Marti et al.⁸ found a nonlinear dependence of friction with applied force. They further found that, for a given applied force, the friction varied with pH in accordance with the change in surface potential. However, in an effort to establish a correlation of friction with adhesion hysteresis, Marti et al.⁸ used the area between the approach and separation force curves to calculate a value for the dissipated energy. They found a quantitative relationship between "adhesion hysteresis" and friction. This finding is difficult to understand because the area between the loading and unloading force curves is dependent upon the stiffness of the AFM cantilever used: it is large for a weak cantilever and small for a stiff cantilever. Obviously, friction should be a property of the surfaces and not of the device used to measure friction. It appears that Marti et al.⁸ have confused the JKR surface-energy hysteresis, identified by Israelachvili and co-workers,^{5,32} with hysteresis due to the force measuring spring.

Our results indicate that friction can exist within the electrical double layer, provided that the energy-transfer processes responsible for friction are significant. Two energy-transfer mechanisms are possible: direct surface-surface interaction and indirect interaction mediated via interstitial water. The results show that the friction becomes negligible at about 0.7 nm, which is before the surfaces are separated by even the size of a water molecule. Further, it appears that the presence of a single layer of *mobile* interstitial water molecules is enough to eliminate friction between the opposite surface atoms. Almost by definition, interstitial water is less strongly bound than either the atoms of the solid or even water in the hydration layer. Hence, the magnitude of the energy transfer between the surface and the mobile water molecules is likely to be small, even though they are in close proximity. This proposal is supported by the findings of Horn et al.,³⁹ who showed through drainage measurements that water molecules retain the properties of bulk water down to a single monolayer. In other words, a single layer of removable water molecules can achieve effective lubrication, in part by separating the solid surfaces by a distance greater than the range of the friction force, but also because the water-surface interactions are weaker than the surface-surface interactions.

Conclusions

It has long been recognized^{32,40,41} that friction between two mutually attractive surfaces experiences an additional component to the frictional force, over and above the effect of applied force. Thus, traditionally, the friction force is expressed as a linear function of the applied force plus the adhesion. In this paper this approach has been extended to nonadhesive surfaces. It was shown that the intrinsic

(39) Horn, R. G.; Smith, D. T.; Haller, W. *Chem. Phys. Lett.* **1989**, *162*, 404.

(40) Derjaguin, B. *Research in Surface Forces*; Consultants Bureau: New York, 1966; Vol. 2.

(41) Dowson, D. *History of Tribology*; Longman: London and New York, 1979.

force was the determinant of friction for both adhesive and nonadhesive surfaces.

Surface separation, rather than the direct effect of applied force, was seen in this study to control friction. The electrical double-layer interactions provided a means to investigate friction as a function of surface separation. Because the interaction force law varied with pH, comparing friction at the same force but at different pH enabled us to distinguish the effect of applied force from the effect of separation. Rather than cause complication, the double-layer interactions have allowed friction to be studied quantitatively while independently varying separation, adhesion, and applied force.

The detachment force, F_{detach} , was shown to be the most important measurable parameter in this study of friction. It was shown that F_{detach} adequately accounts for the variation in interaction force from the electrical double layer (including specific surface chemistry, hydration forces, and other surface forces). From F_{detach} , the intrinsic force is readily calculated; it is the applied force less the detachment force. When the combined effect of F_{detach} and the applied load was plotted as intrinsic force, friction was shown to be a function only of the intrinsic force. This function was independent of pH.

Surface-profile calculations showed that very little elastic deformation occurred under the small applied forces in this study. Theoretical fits to the measured force curves enabled a calculation of separation at resolutions far greater than experiment. As a result, the effect of applied force was seen to control friction indirectly by changing the surface separation. Friction was seen to decrease rapidly at separations away from "soft" contact. This dependence of friction on separation was shown to account for the nonlinear coefficient of friction.

This study has shown that the AFM is an ideal tool for the study of friction forces in aqueous colloidal systems. The measurement of the interaction force law, in addition to the friction force, enables the effects of adhesion and the specific force law on friction to be quantified. In contrast to taking friction measurements in air, conducting the study in aqueous solution has allowed the surface separation, adhesion, and applied force to be controlled independently.

Acknowledgment. A.F. acknowledges the University of South Australia for providing an overseas postgraduate research scholarship. Gerald Belder and Rob Hayes (both of Philips Research, The Netherlands) kindly provided the silica and titanium dioxide wafers. The sputtered coatings and layer-thickness measurements were carried out by ellipsometry at Philips Research (The Netherlands). Bill Skinner (Ian Wark Research Institute, Australia) is thanked for XPS analysis of the titanium dioxide wafer. Anthony O'Dea (Ian Wark Research Institute, Australia) is thanked for help with an automated procedure for the analysis of the friction data. We also thank Roger Horn for helpful discussions. Financial support from the Australian Mineral Industries Research Association (AMIRA) is gratefully acknowledged.

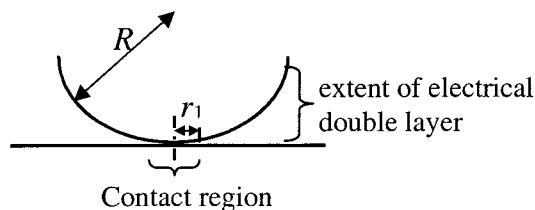


Figure 10. Schematic of the extent of the electrical double layer between a sphere, of radius R , and flat substrate. The contact region of radius r_1 defines the apparent contact area within which electrolyte exists because of surface roughness.

Appendix. Relative Contribution of the Electrical Double Layer within the Contact Region. Figure 10 shows a schematic of a sphere in contact with the substrate. The contact region, radius r_1 , represents the apparent contact area, within which electrolyte exists as a result of surface roughness.⁹ The force, F_1 , due to the double-layer interaction within the contact region of radius r_1 , is calculated according to the conventional double-layer force law as:

$$\begin{aligned} F_1 &= 2\pi \int_0^{r_1} dr r p(h(r)) \\ &= 2\pi \int_0^{r_1} dr_1 r A e^{-\kappa h(r)} \\ &= 2\pi A e^{-\kappa h_0} \int_0^{r_1} dr r e^{-\kappa r^2/2R} \\ &= 2\pi A e^{-\kappa h_0} \int_0^{r_1} dr \frac{d}{dr} e^{-\kappa r^2/2R} \left(\frac{-R}{\kappa} \right) \\ &= \frac{-2\pi AR}{\kappa} e^{-\kappa h_0} (e^{-\kappa r_1^2/2R} - 1) \end{aligned}$$

where A is a constant, R is the radius of the sphere, κ^{-1} is the Debye length, and h_0 is the separation. The total force, F_{tot} , exerted on the sphere is obtained by letting $r_1 \rightarrow \infty$

$$F_{\text{tot}} = \frac{2\pi AR}{\kappa} e^{-\kappa h_0}$$

Therefore, the relative contribution of F_1 to the total force is

$$\frac{F_1}{F_{\text{tot}}} = 1 - e^{-\kappa r_1^2/2R}$$

In the current study, $R = 3.5 \mu\text{m}$, $\kappa^{-1} = 10 \text{ nm}$ (10^{-3} M 1:1 electrolyte), and $r_1 = 0.06 \mu\text{m}$ (estimated by assuming that contact between the surfaces occurred up to a separation of 1 nm). Inserting these values into the last equation gives a relative contribution from the contact region of 5%. Therefore, any contribution of the pH to friction is, in fact, dominated by changes in the double layer outside of the contact region.

LA000881N